PROC. OF JSCE,
No. 292, December 1979

NONLINEAR ANALYSIS OF REINFORCED CONCRETE FRAMES

By Tunwa SIRISREETREERUX and Tada-aki TANABE***

1. INTRODUCTION

(1) Literature Review

The behavior of reinforced concrete frame structures is fundamentally nonlinear since the stress-strain relationship of concrete, as shown in Fig. 1, is not linear especially under high load condition, therefore; the elastic methods of analysis such as slope-deflection, moment distribution, and Castigliano's Theorem, etc; are applicable only for the case of low load condition. Assuming the behavior of the frames to be linear at high load condition, after the yielding of reinforcing steel, produces large amount of error because of the rotations of plastic hinges.

Early research works were mostly on the determination of the rotational capacities of plastic hinges in reinforced concrete members. In 1956, Baker[2] suggested a rather complicated set of equations in terms of the compressive force and section properties. His equations yield a safer prediction of the available plastic rotation than the other methods. In 1966, Corley[16] proposed the equivalent length of the plastic hinge equation in terms of the section properties and steel reinforcement which were based on the test of simply supported beams. Mattock[3] developed Corley's equation to a simple form which fit the experimental data. Sawyer[13] also proposed a simple equation for the length of plastic hinge based on the assumptions that the maximum moment in the member is the ultimate moment and the zone of yielding is spread over one-quarter of the depth of the section past the section in which the bending moment is reduced to yield moment. As for the comprehensive analysis and design procedures to consider moment redistribution in concrete structures, essentially there are two analytic approaches used. That is, the mechanism approach in various forms which is the basis for the three design methods of Sawyer, Baker, and Cohn which have been retained for consideration by the ACI-ASCE Committee 428 on limit design and an analysis by successive linear approximation. Past work in the latter direction has been quite limited, however, for concrete structures. Scordelis and Ngo[1] presented a finite element solution for particular cracking pattern. Ernst and Berwanger[5] showed a modified elastic analysis approach for beams. Wang[6] have developed a general finite element computer program for limit analysis of frames but it lacks the sophistication to handle complicated concrete structures. Lazaro and Richard[4] derived the stiffness matrix using a beam element. In deriving the stiffness of each member, the moments working at both ends were assumed before hand and the overall analysis was repeated until the assumed end moments agree with the resulting end moments. When a certain critical point reaches the stage of plastic hinge, the computer sets up a new nodal point.

(2) Scope of the Study

This study is closely related to the later approach. However, no linear approximation was made. Instead, a set of simultaneous equations of unknown curvatures at each segments are derived applying a simple load-moment-curvature relationship. An iteration is carried out until the resulting curvature agrees with the curvature that is uniquely given by the moment working at the section. In this way, a rigorous method of analysis of reinforced concrete frames which is applicable for all stages of loading (these are the stages after the formation of several hinges until collapse) is formulated. Furthermore, the ultimate load and capacity of plastic hinge rotation is also studied.

2. METHOD OF ANALYSIS

(1) Assumption

The following assumptions are made in the analysis : (1) axial deformation, shear deformation and slenderness effect are neglected, (2) small displace-

* Graduate Student Asian Institute of Technology
** Associate Professor Asian Institute of Technology

ment is assumed, (3) plane sections remain plane after bending, (4) the structures are divided into finite small segments; the curvature along any segment is assumed to be constant.

(2) Stress-strain relationships

The stress-strain relationships of concrete and reinforcing steel in tension and compression adopted in this analysis are as shown in Fig. 1 and Fig. 2, respectively.

(3) Sign convention

Positive sign conventions for moments and shears are as shown in Fig. 4.

(4) Load-moment-curvature relationship of a section

Let the rectangular section shown in Fig. 3 (a) be subjected to axial force P and bending moment M, and let the strain distribution across the section be linear as in Fig. 3 (b). The stress distribution in the concrete and steel corresponding to the strain can be evaluated according to the stress-strain characteristic of the concrete and steel mentioned in item **2.(2)** as shown in Fig. 3 (c). The load-moment-curvature relationship can be generated as follows:

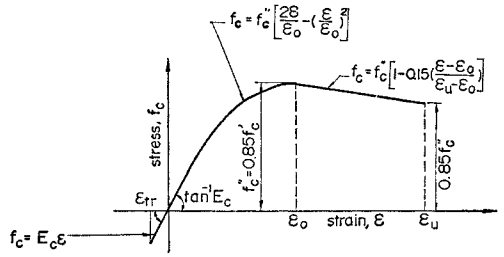

Fig. 1 Assumed Stress-Strain Curve for Concrete.

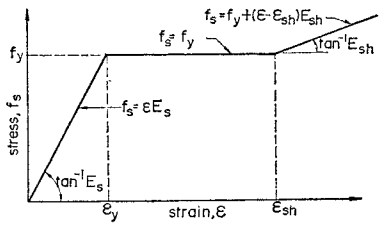

Fig. 2 Assumed Stress-Strain Curve for Steel.

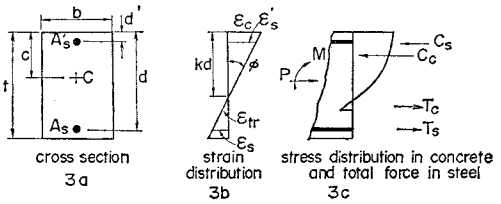

Fig. 3 Stress-Strain Distribution in Section.

$$P=\frac{bkd}{\varepsilon_c}\int_{\varepsilon_{tr}}^{\varepsilon_c} f_c(\varepsilon)\,d\varepsilon+f_s(\varepsilon_s')A_s'-f_s(\varepsilon_s)A_s \quad \cdots\cdots(1)$$

$$M=b\left(\frac{kd}{\varepsilon_c}\right)^2\int_{\varepsilon_{tr}}^{\varepsilon_c} f_c(\varepsilon)\varepsilon\,d\varepsilon+f_s(\varepsilon_s')A_s'(kd-d') +f_s(\varepsilon_s)A_s(d-kd)-P(kd-c) \quad \cdots\cdots(2)$$

$$\phi=\frac{\varepsilon_c}{kd} \quad \cdots\cdots(3)$$

where the symbols are defined in Fig. 3, $f_c=f_c(\varepsilon)$ and $f_s=f_s(\varepsilon)$ represent the stress-strain characteristics of the concrete and reinforcing steel as in Fig. 1 and Fig. 2, respectively.

Equations (1) and (2) are nonlinear; usually, a closed form solution cannot be expected. Therefore; a numerical iterative method of solution is developed. In this method P and ε_c are assumed and the corresponding k and M values are calculated. The strain ε_c is increased monotonically and at each ε_c value, a "k" value is found by iteration to satisfy the force equilibrium of equation (1). The moment, M is calculated from the moment equilibrium of equation (2) and ϕ is determined by equation (3). In this way, the moment, axial force, strains and stresses, corresponding to any deformation imposed on the section, are found. The results are expressed in terms of the continuous load-moment-curvature diagram. The flow chart for the basic steps of the numerical method adopted here is shown in Fig. 6.

(5) Slope-deflection relation

Consider the elastic curve shown in Fig. 5, with the left end of the member as the origin of the X axis directed along the original undeflected position of the straight member, and the Y axis directed

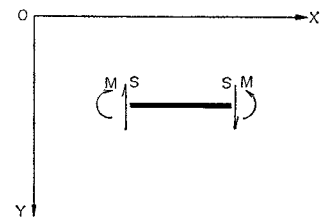

Fig. 4 Positive Sign Conventions for Moments and Shears.

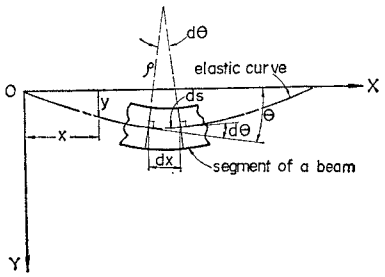

Fig. 5 Elastic Curve.

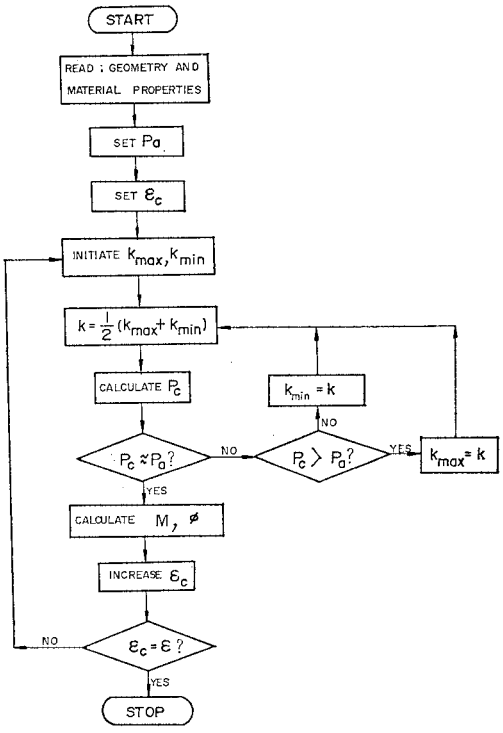

Fig. 6 Flow Chart for the Numerical Method of Analysis for M-ϕ Curve.

positive downward. The deflections are assumed to be so small that there is no appreciable difference between the original length of the member and the projection of its deflected length. Consequently, the curve is very flat and its slope at any point is very small. Hence,

$$\frac{d^2y}{dx^2}=-\phi(x) \quad \cdots\cdots(10)$$

where $\phi(x)$ is the curvature per unit length of member at any point X and assumed positive when concave upward as shown in Fig. 5.

Integrating equation (10) twice leads to

$$\frac{dy}{dx}=-\int \phi(x)\,dx+C_1 \quad \cdots\cdots(11)$$

and

$$y=-\iint \phi(x)\,dx\,dx+C_1X+C_2 \quad \cdots\cdots(12)$$

where C_1 and C_2 are arbitary constants of integrations. Equations (11) and (12) are the standard expressions for the slope and deflection. For a member n divided into N small segments of width ΔX, by virtue of the assumptions made earlier, equations (11) and (12) can be written in numerical forms as,

$$(dy/dx)_{n,m}=-\sum_{i=1}^{m}\phi_{n,i}(x)\,\Delta x_{n,i}+C_{n,1} \quad \cdots\cdots(13)$$

and

$$Y_{n,m}=-\sum_{i=1}^{m}\sum_{j=1}^{i}\phi_{n,j}(x)\,\Delta X_{n,j}\Delta X_{n,i}+C_{n,1}X+C_{n,2} \quad \cdots\cdots(14)$$

where,

$(dy/dx)_{n,m}$=slope or rotation at segment m of member n

$Y_{n,m}$=deflection at segment m of member n

$\phi_{n,i}(x)$, $\phi_{n,j}(x)$=curvature at segments i and j, respectively; of member n

$\Delta X_{n,i}$, $\Delta X_{n,j}$=width of segments i and j, respectively, of member n

$C_{n,1}$, $C_{n,2}$=first and second integration constants, respectively; of member n

and

$$1\leq m\leq N \quad \cdots\cdots(15)$$

(6) Simultaneous equations

By using $\phi(x)$ as the unknown variable, if the number of $\phi(x)$ of all members is N then a set of N simultaneous equations are needed for solving the values of N unknowns. All these equations can be generated by equilibrium, compatibility and boundary conditions.

a) Equilibrium of forces at the segment

The equilibrium of forces at any segment and equilibrium of moments at any joint must be satisfied.

By definition,

$$S(x)=\frac{dM(x)}{dx} \quad \cdots\cdots(16)$$

where

$S(x)$=shearing force at point x

$M(x)$=bending moment at point x

For numerical computation, equation (16) can be written as

$$S(x)=\frac{M(x+\Delta x)-M(x)}{\Delta x} \quad \cdots\cdots(17)$$

Therefore;

$$S_{n,m}=\frac{M_{n,m+1}-M_{n,m}}{\Delta X_{n,m}} \quad \cdots\cdots(18)$$

where,

$S_{n,m}$=shearing force at segment m of member n

$M_{n,m}$=bending moment at segment m of member n

$M_{n,m+1}$=bending moment at segment $m+1$ of member n

$\Delta X_{n,m}$=width of segment m of member n

Considering the equilibrium of forces at segment m of member n as shown in Fig. 8,

$$S_{n,m}-S_{n,m+1}=F_{n,m} \quad \cdots\cdots(19)$$

where

$F_{n,m}$=applied load on segment m of member n.

Substituting equation (18) into equation (19) leads to

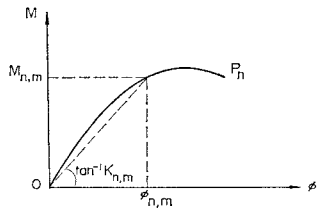

Fig. 7 M-ϕ Curve.

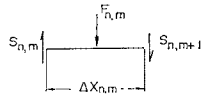

Fig. 8 Equilibrium of Forces at Segment.

$$\frac{M_{n,m+1}-M_{n,m}}{\Delta X_{n,m}}-\frac{M_{n,m+2}-M_{n,m+1}}{\Delta X_{n,m+1}}=F_{n,m} \quad \cdots\cdots(20)$$

If $\Delta X_{n,m}$ in equation (20) is equal to $\Delta X_{n,m+1}$, $\Delta X_{n,m+2}$ and so on, equation (20) becomes

$$-M_{n,m}+2M_{n,m+1}-M_{n,m+2}=F_{n,m}\Delta X_n \quad \cdots\cdots(21)$$

where

ΔX_n = width of segment of member n.

Now, from the relationship between M and ϕ in Fig. 7 and by geometry,

$$M_{n,m}=K_{n,m}\phi_{n,m} \quad \cdots\cdots(22)$$

where $K_{n,m}$ is the total flexural stiffness at segment m of member n. Substituting equation (22) into equation (21) yields

$$-K_{n,m}\phi_{n,m}+2K_{n,m+1}\phi_{n,m+1}-K_{n,m+2}\phi_{n,m+2}=F_{n,m}\Delta X_n \quad \cdots\cdots(23)$$

Equation (23) is the force equilibrium at segment m of member n.

b) Equilibrium of moments at joint

Considering the equilibrium of moments at joint O as shown in Fig. 9,

$$M_{n1,m1}+M_{n2,m2}+M_{n3,m3}+M_{n4,m4}=0 \quad \cdots(24)$$

where $M_{n1,m1}$, $M_{n2,m2}$, $M_{n3,m3}$ and $M_{n4,m4}$ are the moments of members $n1$, $n2$, $n3$ and $n4$, respectively; at the segments vicinity of joint O.

Substituting equation (22) into equation (24) leads to

$$K_{n1,m1}\phi_{n1,m1}+K_{n2,m2}\phi_{n2,m2}+K_{n3,m3}\phi_{n3,m3}+K_{n4,m4}\phi_{n4,m4}=0 \quad \cdots\cdots(25)$$

Equation (25) is the moment equilibrium at the joint.

c) Compatibility and boundary condition

The constant $C_{n,1}$ and $C_{n,2}$ in equations (13) and (14) can be determined from the boundary conditions

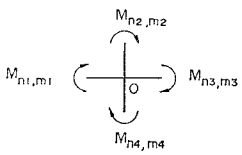

Fig. 9 Equilibrium of Moments at Joint.

or by the compatibility at the ends of the member. Hence, by means of equilibrium, compatibility and boundary condition as mentioned, a set of simultaneous equations can be generated for solving all unknowns and this may be written in the matrix form as

$$[K]\{\phi\}=\{F\} \quad \cdots\cdots(26)$$

where

$\{F\}$ = structural column matrix of external applied loads

$\{\phi\}$ = structural column matrix of segment curvatures

$[K]$ = structural stiffness matrix and is a function of $\{\phi\}$

(7) Interative process of solution

Since equation (26) is nonlinear, a direct method of solving the unknowns cannot be used; therefore, an iterative method is needed. The steps involved in solving for unknowns are described below and the corresponding flow chart is shown in Fig. 10.

1. Assume all values of axial forces (P_a) and segment curvatures (ϕ_a); elastic values are recommended.
2. Develop P-M-ϕ curves for all members by using the values of axial forces (P_a) in 1.
3. Determine the values of $K_{n,m}$ corresponding to ϕ_a and P-M-ϕ curves in 1 and 2, respectively.
4. Set equation $[K]\{\phi\}=\{F\}$ as in equation (26) and solve for the unknown (ϕ_c).
5. Compare the values ϕ_a and ϕ_c

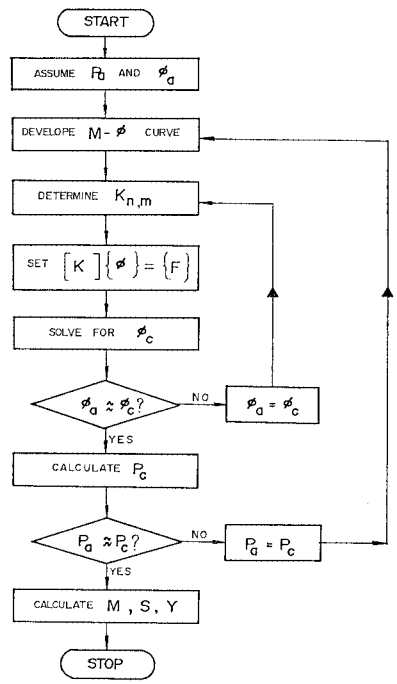

Fig. 10 Flow Chart for Iterative Process.

If ϕ_a is not close enough to ϕ_c then change the values of ϕ_a to ϕ_c and go to step 3.

If ϕ_a is close enough to ϕ_c then calculate the values of all axial forces (P_c).

6. Compare the values of P_a and P_c

If P_a is not close enough to P_c then change the values of P_a to P_c and go to step 2.

If P_a is close enough to P_c then determine every required values, i.e.; $M_{n,m}$, $S_{n,m}$, $Y_{n,m}$.

3. COMPARISON OF THE EXPERIMENTAL RESULTS WITH THE RESULTS OF THE PRESENT STUDY

To compare the experimental results and numerical results of this study, several cases were studied.

(1) Case 1

Three two-span continuous beams 8 EI, 16 EI and 27 EI subjected to two point loads at midspans as shown in Fig. 11 were analyzed, experimental result of which were quoted from Reference No. 10. The section and material properties used are shown in Table 1. The moment distribution at each load

Table 1 Section Details and Material Properties for Example 1.

	Unit	Beam 8 EI	Beam 16 EI	Beam 27 EI
t	in	14.5	14.5	14.5
b	in	6.0	6.0	6.0
d	in	12.5	12.5	12.5
d'	in	2.0	2.0	2.0
A_s	in^2	0.62	1.2	2.0
A_s'	in^2	0.62	1.2	2.0
f_c'	lb/in^2	5 280	5 280	5 280
E_c	lb/in^2	4.05×10^6	4.05×10^6	4.05×10^6
ε_u	—	0.0038	0.0038	0.0038
ε_{tr}	—	0	0	0
f_y	lb/in^2	42 400	42 600	38 300
E_s	lb/in^2	29×10^6	29×10^6	29×10^6
E_{sh}	lb/in^2	0.769×10^6	0.98×10^6	0.911×10^6
ε_{sh}	—	0.0078	0.0102	0.0090

Table 2 Comparison of Ultimate Loads for Example 1.

Beam No.	Total load on beam, kip		Error (%)
	Test	Proposed method	
8 EI	56.2	48.0	15
16 EI	92.0	81.0	12
27 EI	110.0	117.2	7

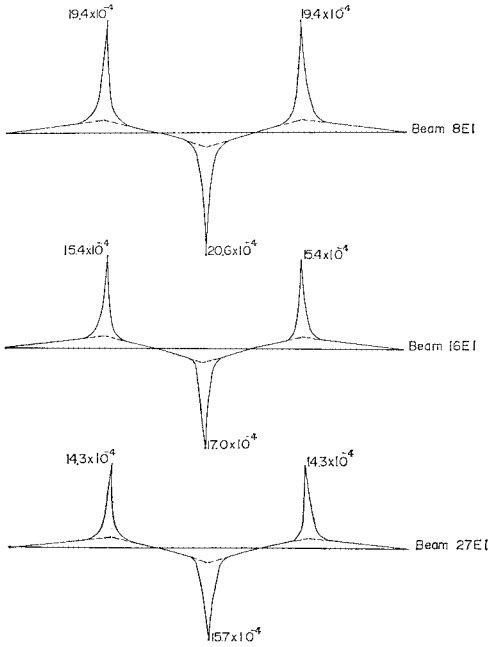

Fig. 12 Curvature Diagrams at Ultimate Loads (Unit : in^{-1} or 0.4 cm^{-1}).

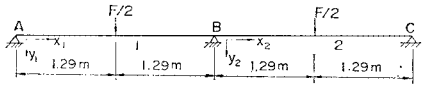

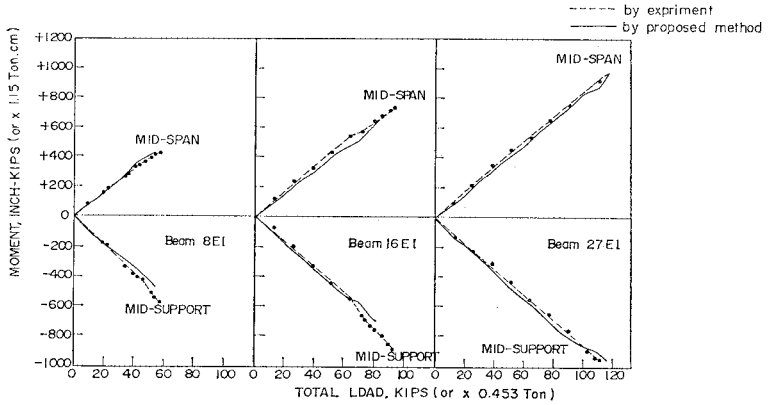

Fig. 11 Distribution of Moments at Loads and Mid-Support in Example 1.

stage and ultimate loads are compared as shown in Fig. 11 and Table 2. The curvature diagrams at ultimate loads are also shown in Fig. 12.

In the first place, the close agreement of moment distribution between the experimental and the theoretical results at loading stages prior to the ultimate stage is noted in Fig. 11. Fig. 13 shows an example of numerical results of the process of moment distribution after the initiation of a plastic hinge. In the case of Beam 27 EI, it is noted that at the load of $F/F_u=0.80$ yielding of the mid-support start and at the load of $F/F_u=0.87$ yielding of mid-span also start and the formations of three plastic hinges proceed almost simultaneously. When the mid-support reaches its ultimate capacity, the mid-span reaches the 91 percent of its ultimate capacity. Depending upon the span ratio loading conditions and so forth, the process of formation of plastic hinges are quite different and present study is possible to clearly analize the difference of those processes.

While the general trends obtained by the proposed method are in good agreement with those obtained by the experiments[10] there exist some differences of the ultimate values of the mid-support moment in 8 EI and 16 EI beams. The ultimate loads for beams 8 EI, 16 EI and 27 EI in Table 2 show the differences of about 15%, 12% and 7%, respectively. These differences are considered to be due to the failure condition that is, the ultimate strain of the concrete assumed in the analysis and also due to the assumption of analysis that the beam is supported by points instead of supports with certain width which is the case of the experiment and also due to experimental errors since in the experiments the observed ultimate moment of the section at mid-supports are shown to be 15 to 20% larger than the ultimate capacity calculated which are extremely rare when the sectional dimensions and material property are given accurately in view of the study of Hognestad[4].

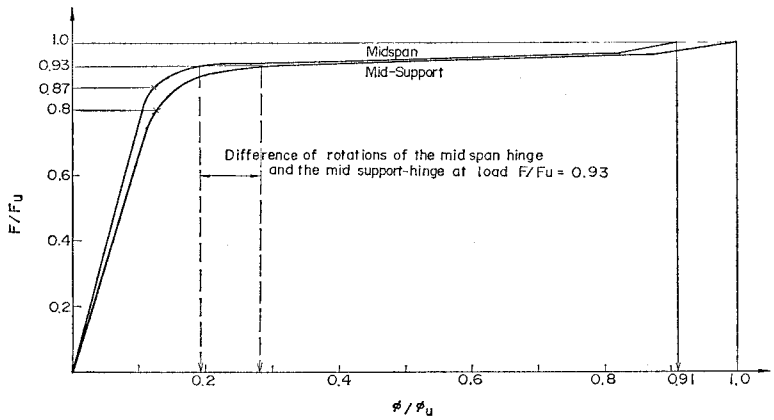

Fig. 13 Load-Curvature Relationships at Critical Sections for Beam 27 EI.

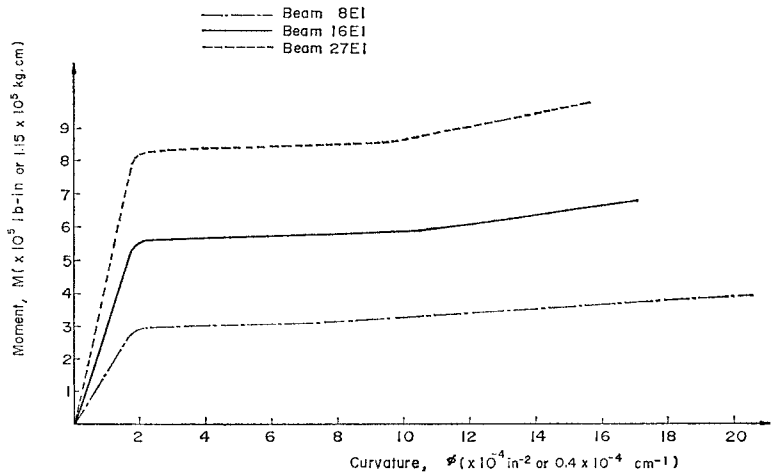

Fig. 14 Moment Curvature Relationship at Ultimate Loads.

From Fig. 12 in combination with Fig. 14, it is possible to obtain the rotational capacity of a plastic hinge just at the collapse of the continuous beams and also the amount of moment redistribution.

For above three continuous beams, the redistribution of negative moments at mid-support is found to be about 13%. In these cases both the mid-support section and the load sections reached the plastic hinge condition without so much redistribution of moments.

(2) Case 2

A portal frame C 1 subjected to a horizontal point load as shown in Fig. 15 is analyzed by the proposed method, experimental result of which is quoted from Reference No. 8. The section details and material properties are tabulated in Table 3. The load is increased up to ultimate. The ultimate load capacity

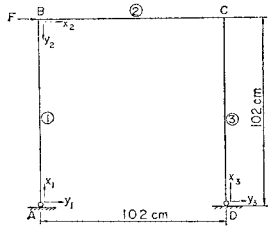

Fig. 15 Frame in Example 2.

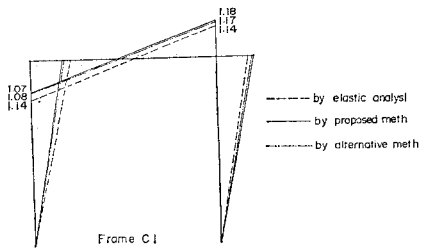

Fig. 16 Moment Redistribution (kip-ft or 0.138 t-m) Ultimate Load of Example 2.

Table 3 Section Details and Material Properties for Example 2.

	Unit	Frame C 1		Unit	Frame C 1
t	in	4.0	E_c	lb/in²	3.5×10^6
b	in	3.0	ε_u	—	0.0038
d	in	3.25	ε_{tr}	—	0
d'	in	0.75	f_y	lb/in²	45 000
A_s	in²	0.1	E_s	lb/in²	29×10^6
A_s'	in²	0.1	E_{sh}	lb/in²	0
f_c'	lb/in²	3650	ε_{sh}	—	—

Table 4 Comparison of Ultimate Load for Example 2.

Frame No.	Ultimate Load, lb		Error (%)
	Experiment	Proposed Method	
C 1	693	710	2.5

and load-deflection curve compared with the experimental values[8] are shown in Table 3 and Fig. 17, respectively, which show the close agreement of compared values. The distribution of bending moment at ultimate load compared with elastic analysis is shown in Fig. 16. The curvature diagram at ultimate load is shown in Fig. 18.

The proposed method gives results which are very close to the experimental result since the difference of ultimate loads is only 2.5%. Fig. 16 shows the distribution of moments at ultimate load, the moments at joints B and C are about 6% less and 4% more respectively than the elastic values. The difference of these two moments from the elastic analysis is due to the effects of axial forces on the sectional stiffnesses of columns AB and CD. Applied lateral force F causes column CD to be stiffer than column AB, since the column AB is in tension while column CD is in compression. Hence, the moment at joint C is greater than that at joint B.

In Fig. 17, the load-deflection relationship was compared. It is to be noted that in the present study, good prediction of the real behavior of the frame is achieved. In Fig. 18 and Fig. 19, the

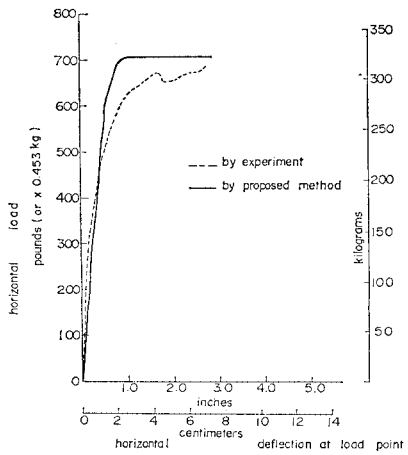

Fig. 17 Load-Deflection Curve for Example 2.

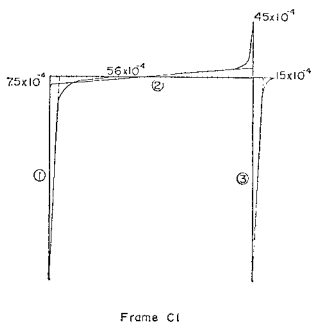

Fig. 18 Curvature Diagram at Ultimate Load (by in^{-1} unit or 0.4 cm^{-1}).

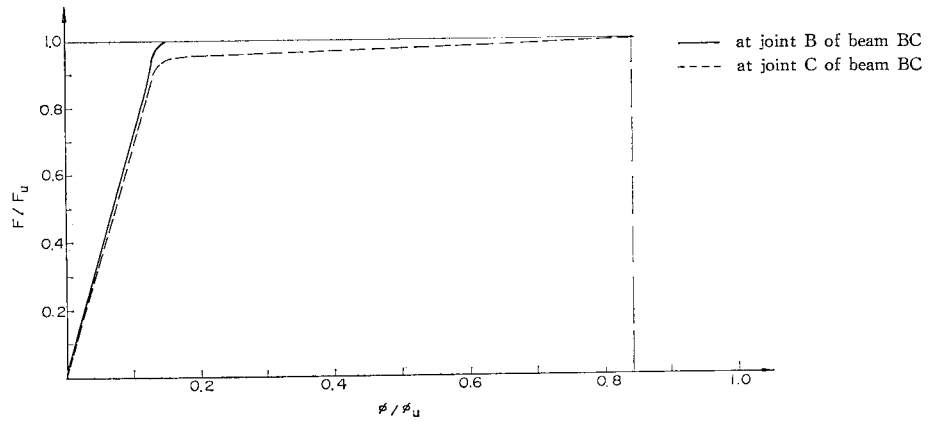

Fig. 19 Load-Curvature Relationship at Ultimate Load for Frame C1.

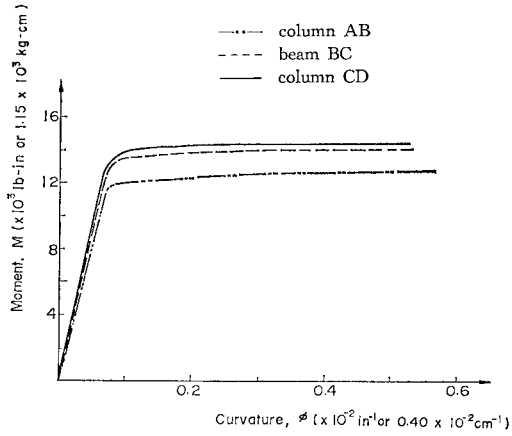

Fig. 20 Load-Moment-Curvature Relationships at Ultimate Load for Frame C1.

curvatures at ultimate load are shown. Furthermore, it is interesting to note that at a joint of a beam and a column, the curvatures are quite different for a beam and a column even though they have the same amount of moments and final failure is controled by the failure of the column top which is receiving tensile axial force, at which point about 80 percent of the rotational capacity is consumed at one of the beam ends and almost zero in the other end.

(3) Case 3

Two portal frames A 40 and A 60 subjected to two equal vertical, point loads as shown in Fig. 21 are analyzed, experimental result of which is quoted from Reference No. 11. The section details and material properties are shown in Table 5. The loads are increased up to ultimate. The load-midspan deflection curves and ultimate capacities of the frames compared with the experiments are shown in Fig. 22 and Table 6, respectively. The distribution of moment at ultimate loads compared with elastic analysis are shown in Fig. 23, and the curvature diagrams at ultimate loads are shown in Fig. 24.

The load-capacities of the frames shown in Table 6 and the load-deflection curves shown in Fig. 22 indicate that the results obtained by the proposed method are in very good agreement with those obtained experimentally since the difference in ultimate loads is only 1.3%. It can be seen from Fig. 23 that the negative moments at the joints of frames A 40 and A 60 are about 0.3% and 0.4%, greater

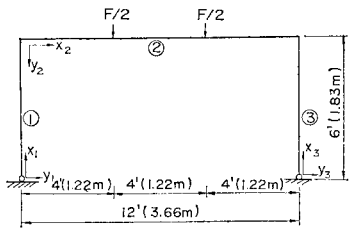

Fig. 21 Frame in Example 3.

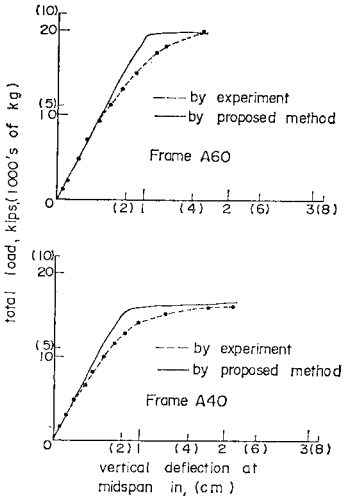

Fig. 22 Load-Deflection Curves for Example 3.

Table 5 Section Details and Material Properties for Example 3.

	Unit	Frame A 40	Frame A 60
t	in	8.0	8.0
b	in	4.5	4.5
d	in	6.5	6.5
d'	in	1.5	1.5
A_s	in^2	0.62	0.62
A_s'	in^2	0.62	0.62
f_c'	lb/in^2	4 220	5 650
E_c	lb/in^2	4.05×10^6	4.05×10^6
ε_u	—	0.0038	0.0038
ε_{tr}	—	0	0
f_y	lb/in^2	51 200	61 700
E_s	lb/in^2	29×10^6	29×10^6
E_{sh}	lb/in^2	0.86×10^6	1.68×10^6
ε_{sh}	—	0.015	0.0068

Table 6 Comparison of Ultimate Loads for Example 3.

Frame No.	Total load, kip		Error (%)
	Experiment	Proposed method	
A 40	15.9	16.1	1.3
A 60	19.96	19.7	1.3

respectively, while the positive moments at midspan are about 5.9% and 6.5% less respectively, than the moments obtained by elastic analysis which indicates that the negative and positive moments are identical. This is due to the effect of compressive axial forces in the columns which causes the increase in the stiffness of the columns. In Fig. 24 and Fig. 25 (a), the curvatures at ultimate loads are shown. It is to be noted that at ultimate stages the curvature at midspan of the beam is approximately one-half of that at the column face of the beam.

4. ANALYSIS OF A MULTISTORY FRAME

A multistory frame subjected to three equal horizontal point loads as shown in Fig. 27 is studied. The section details and material properties used are tabulated in Table 7. The distribution of bending moments are compared with elastic analysis as shown in Fig. 29.

The same frame subjected to uniform vertical loads as shown in Fig. 28 is also analyzed. The

Table 7 Section Details and Material Properties for Multistory Frame.

	Unit	Dimension		Unit	Dimension
t	cm	40	E_c	kg/cm^2	0.24×10^6
b	cm	20	ε_u	—	0.0038
d	cm	35	ε_{tr}	—	—
d'	cm	5	f_y	kg/cm^2	3 000
A_s	cm^2	10	E_s	kg/cm^2	2.1×10^6
A_s'	cm^2	10	E_{sh}	kg/cm^2	—
f_c'	kg/cm^2	350	ε_{sh}	—	—

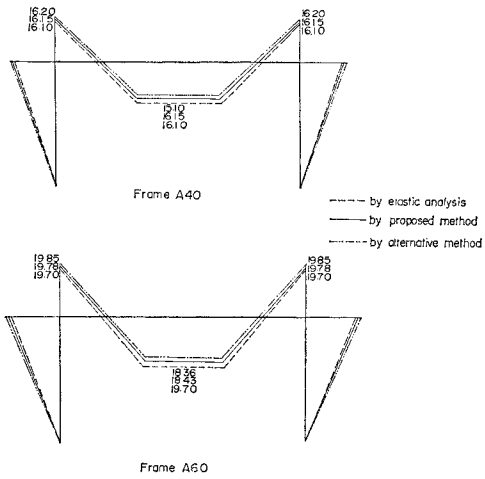

Fig. 23 Moment Distribution (kip-ft or 0.138 t-m) at Ultimate Loads of Example 3.

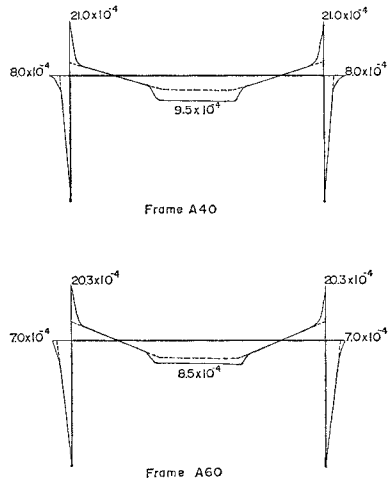

Fig. 24 Curvature Diagrams at Ultimate Loads (ϕ by in^{-1} or 0.40 cm^{-1}).

distribution of moments compared with elastic analysis are shown in Fig. 30 and Fig. 31 for two sets of loadings.

The maximum difference in the moments obtained from elastic analysis is 6% for lateral loading and 15% for vertical loading. Because of the rough discretization used, the numerical results show some error. Without this error, the difference would amount to several percent or more according to the section properties of the elements.

5. ALTERNATIVE METHOD OF REINFORCED CONCRETE FRAME ANALYSIS

Since it is found from the present study that the

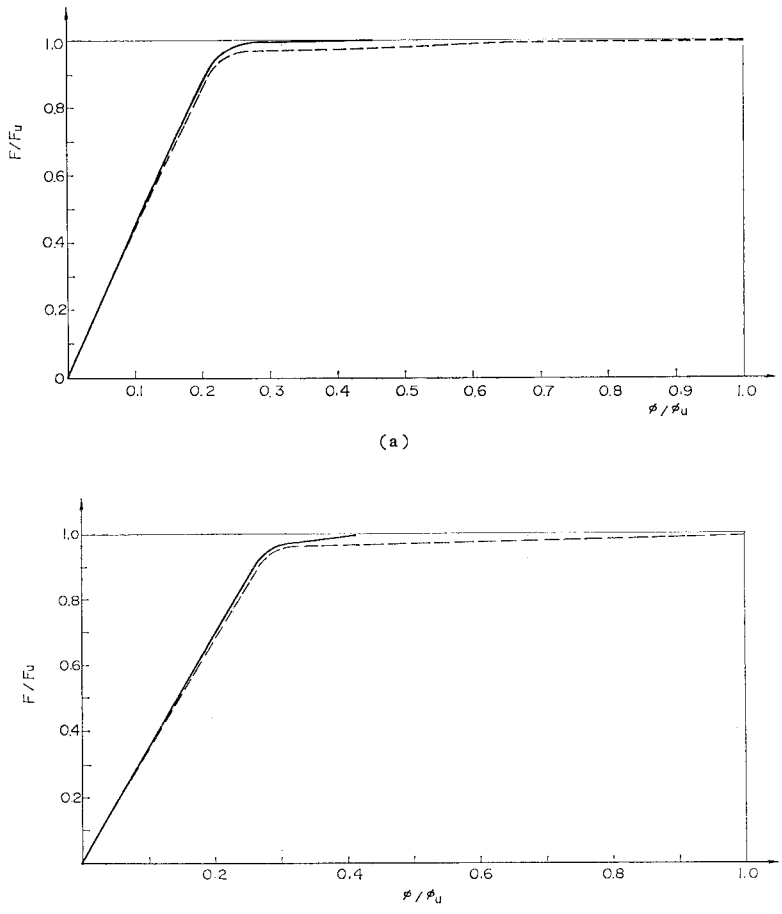

Fig. 25 Load-Curvature Relationships at Critical Sections of the beam for Frame A 40.

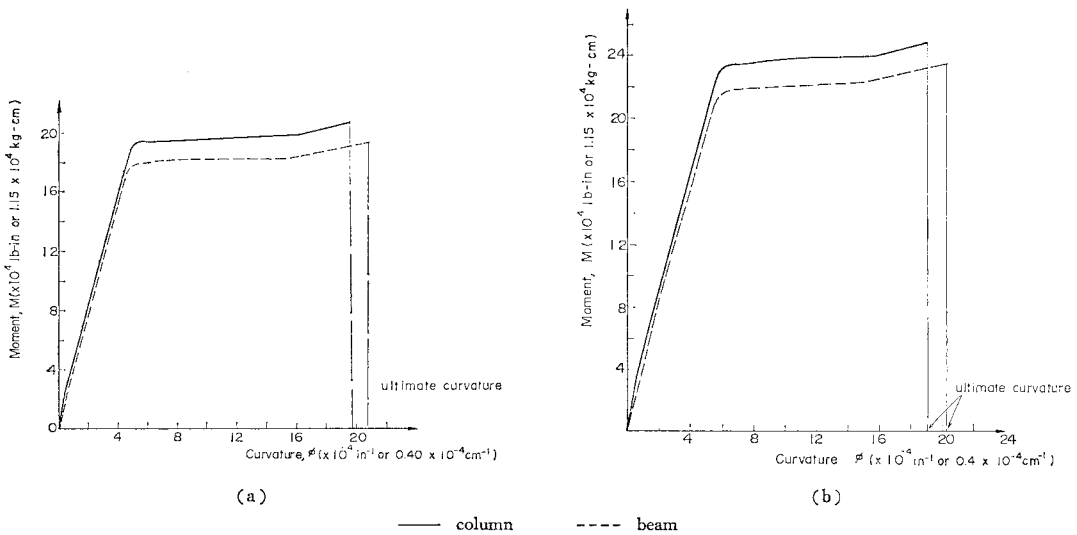

Fig. 26 Load-Moment-Curvature Relationships at Ultimate Load for Frame A 40.

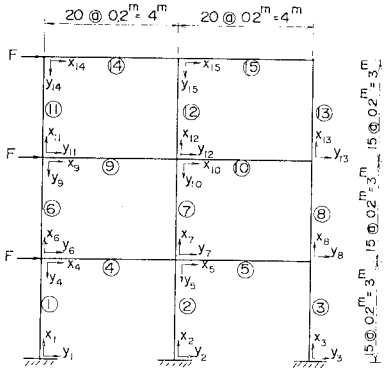

Fig. 27 Multistory Frame Subjected to Lateral Loads.

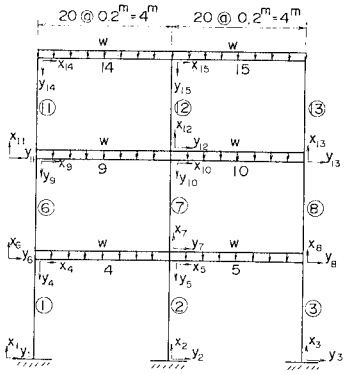

Fig. 28 Multistory Frame Subjected to Vertical Loads.

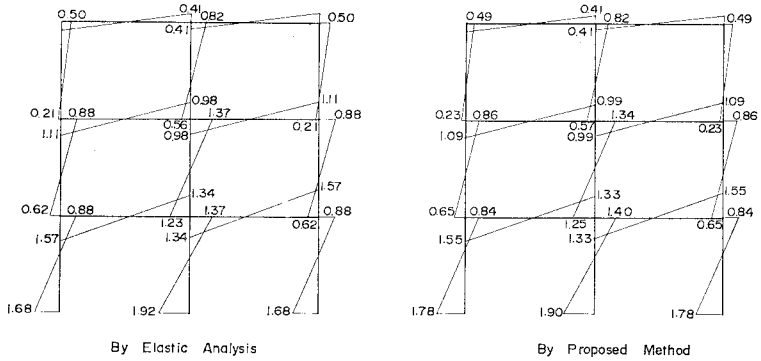

Fig. 29 Bending Moment Diagrams (t-m) Due to Lateral Loads, F=1 t.

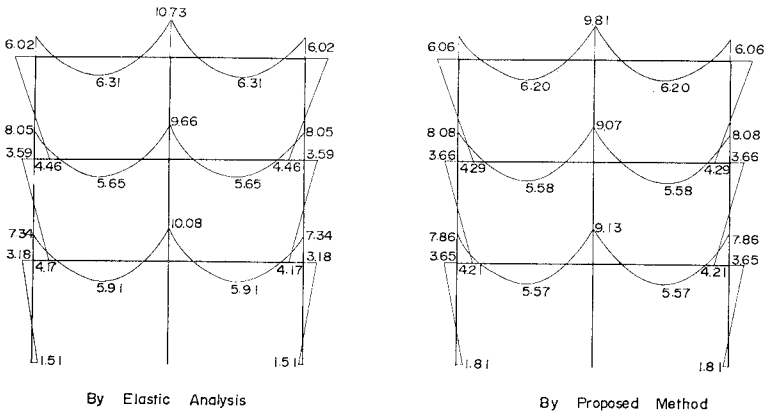

Fig. 30 Bending Moment Diagrams (t-m) Due to Vertical Loads, W=78 kg/cm.

nonlinearity of reinforced concrete frames are mainly due to the axial load effect on column stiffness and rotation after the yielding of steel at a critical section, an alternative elastic method of frame analysis may be used in which the EI to be used in the moment distribution is expressed as a function of P/P_{max} at the loading stage prior to the formation of plastic hinges.

In Fig. 32, the EI values are calculated for the section shown in the same figure for various P/P_{max} values and in Fig. 33 non dimentionalized EI values are shown for each steel amount ratio ranging from ρ=0.01 to ρ=0.08, sectional dimension of which is also shown in the same figure to generalize the discussion. It is to be noted from these figures that $EI/EI_{cracked}$ is roughly approximated by the parabolic function of P/P_{max}.

Hence;

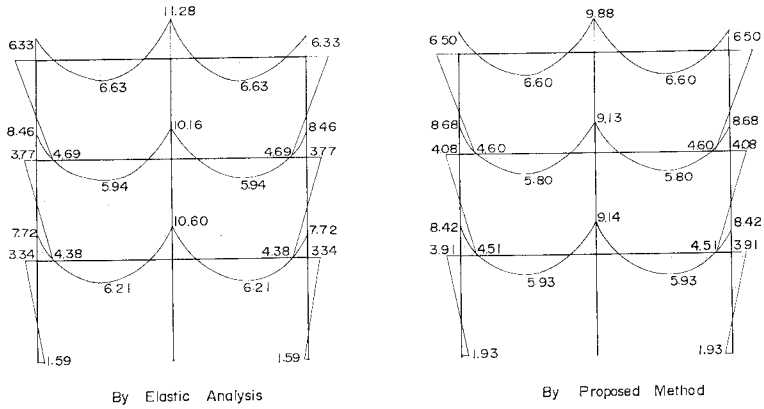

Fig. 31 Bending Moment Diagrams (t-m) Due ot Vertical Loads, W=82 kg/cm.

$$EI/EI_{cracked}=a\left(\frac{P}{P_{max}}\right)^2+b\left(\frac{P}{P_{max}}\right)+c \quad \cdots\cdots(27)$$

where

EI=equivalent flexural stiffness of the section

$EI_{cracked}$=flexural stiffness of the cracked section

P=axial force on the section

P_b=axial force at balanced condition

P_{max}=maximum axial force that the section can take

In view of practical proposes, it would be more useful to obtain the coefficient of Eq. 27 which is applicable to general cases. As three coefficients are necessary three conditions are needed. For this purpose, it is assumed that at P=0, EI=$EI_{cracked}$ and at $P=P_{max}$, EI=0 and EI become maximum at $P=P_b$. The former two assumptions may be justified considering the initial and ultimate conditions of beams and columns. The last assumption is obtained from the numerical results which are shown

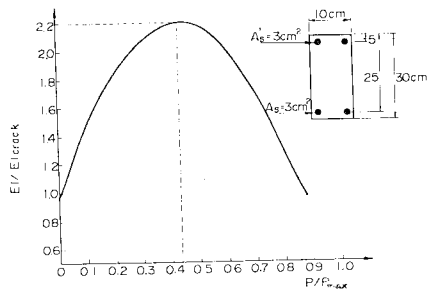

Fig. 32 Relationships between $EI/EI_{cracked}$ and P/P_{max}.

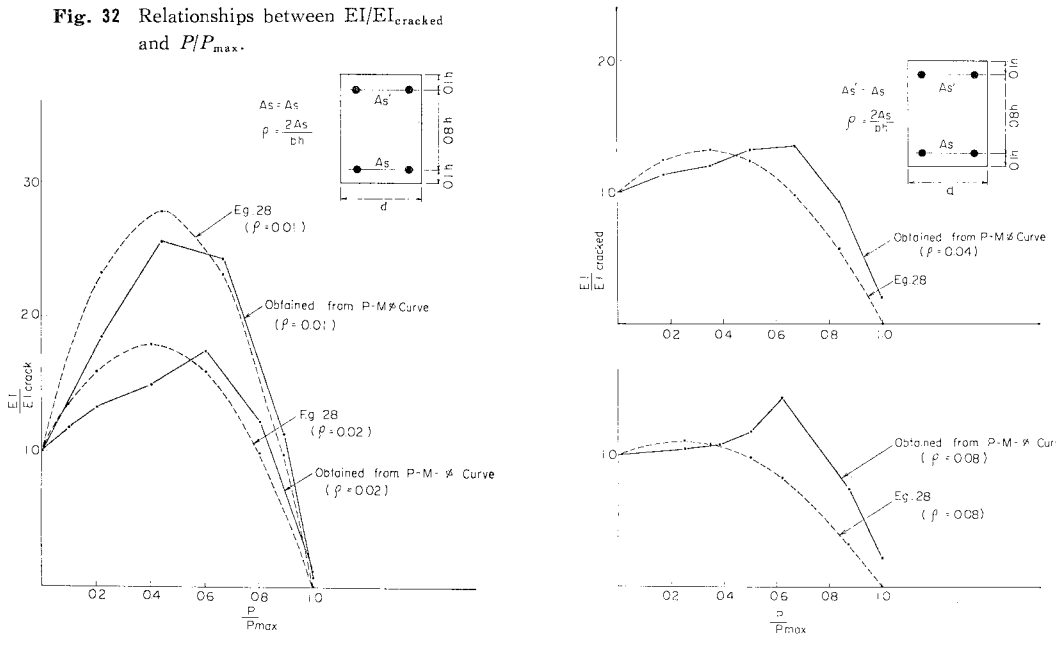

Fig. 33 Fitting of Parabolic Curve to the Rigidity Change.

in Fig. 33. It is noted that EI is always nearly maximum when P equalts the balanced load, P_b.

Then EI is expressed as

$$EI=EI_{cracked}\left[\frac{\left(1.0-\frac{P_b}{P_{max}}\right)^2}{1.0-2.0\frac{P_b}{P_{max}}}-\frac{1.0}{1.0-2.0\frac{P_b}{P_{max}}}\cdot\left(\frac{P}{P_{max}}-\frac{P_b}{P_{max}}\right)^2\right] \quad \cdots\cdots(28)$$

This EI is an approximated value, so gives some inaccuracy. However, using this EI will give much higher accuracy than to use the gross sectional EI in the analysis of frames.

Using equivalent flexural stiffness of the sections (EI) in Eq. (28), the elastic analysis of the frame shown in Fig. 15 and the frame shown in Fig. 21 were carried out. The numerical results were shown in Fig. 16 and Fig. 23 respectively. It was found that the analysis produces small error, as about 1% for examples 2 and 3.

For the moment distribution which exceeds the yielding moment, the rotational capacity should be taken into consideration.

Fig. 12, Fig. 18, and Fig. 24 show the curvature diagrams at ultimate loads of examples 1, 2 and 3 respectively. It is observed from these figures that the shape of curvature diagrams at plastic hinges are always approximately triangular at negative moment area where elastic moment changes sharply. Hence, the plastic hinge rotation at the critical section excluding the effect of diagonal tension cracks may be roughly expressed as :

$$\theta_u=\frac{1}{2}\Delta l(\phi_u-\phi_y) \quad \cdots\cdots(29)$$

where

θ_u=capacity of plastic hinge rotation

ϕ_u=ultimate curvature of the section

ϕ_y=curvature at initial yielding of the steel

Δ_l=width of plastic hinge

The width of plastic hinge, Δ_l, which depends on the material and section properties, configuration of the structures and loading conditions may be roughly approximated by the depth of the section for continuous member and one-half of the depth for discontinuous member.

If we want accurate analysis including the checking of critical rotational capacities we can recourse to the aforementioned analysis.

Conclusively, notwithstanding the fact that the nonlinear properties of concrete and steel exists, an elastic moment distribution may be used up to a load limit at which the steel reaches yielding point at a first critical section. Beyond this load, the redistribution of moment starts. The degree of redistribution of moment depends upon the rotational capacity whose limit is roughly estimated by Eq. (29).

6. CONCLUSIONS

From the result of the study, the following conclusions may be made :

(1) Within the limit of the stated assumptions, the method presented in this study gives reasonably accurate prediction of the deflection and the moment distribution for the whole loading history.

(2) The conventional elastic calculation which is used in design work predicts moments within permissible error for horizontal loading. However, for the loading condition in which pronounced effect of axial load exists, it is necessary to consider the load effect on relative rigidity of members. One way of incorporating this effect is proposed in equation (28). Hence, with the proposed EI value, an elastic moment distribution may be used as an alternative to the iterative method of the present study.

(3) The rotational capacity is relatively small in frame joints than in continuous beam joints and there exist a trend that the capability of the moment redistribution is smaller in frames than in continuous beams if the ultimate concrete strain is kept at around 0.3 percent.

LIST OF SYMBOLS

A_s=area of reinforcing steel in tension,

A_s'=area of reinforcing steel in compression,

b=width of rectangular cross section,

d=effective depth of tension reinforcement,

d'=effective depth of compression reinforcement,

$(dy/dx)_{n,m}$=slope at the middle point of segment m of member n,

E_c=initial tangent modulus of elasticity of concrete,

E_s=modulus of elasticity of steel,

E_{sh}=slope of stress-strain curve for stee in strain-hardening zone,

$F_{n,m}$=applied loads on segment m of member n,

f_y=yielding stress of reinforcing steel,

f_c'=compressive strength of concrete,

$K_{n,m}$=total flexural stiffness at segment m of-member n,

kd=distance from extreme compressive fiber to neutral axis,

$M_{n,m}$=bending moment at segment m of member n,

P_n=axial force in member n,

$S_{n,m}$=shearing force at segment m of member n,

t=total depth of rectangular cross section,

$Y_{n,m}$=deflection at the middle point of segment

m of member n,

$\phi_{n,m}$=curvature at segment m of member n,

$\Delta X_{n,m}$=width of segment m of member n,

ε_c=concrete strain at the extreme compressive fiber of section,

ε_s=strain of tension reinforcement,

ε_s'=strain of compression reinforcement,

ε_{sh}=strain at initiation of strain-hardening of steel,

ε_{tr}=ultimate concrete strain in tension,

ε_u=ultimate concrete strain in compression,

ε_y=strain at initiation of yielding of steel,

REFERENCES

1) Scordelis, A.A. and D. Ngo : Finite Element Analysis of Reinforced Concrete Beams, Journal of A.C.I., Vol. 64, Mar., 1967.
2) Baker, A.L.L. : The ultimate-load theory applied to the design of reinforced and preinforced concrete frames, Concrete Publications Limited,London.
3) Mattok, A. H. : Rotational Capacity of Reinforced Concrete Beams, ASCE journal, V. 93, pp. 519~522, 1967.
4) Angel L. Lazaro, III and Rowland Richards, Jr. : Full-range Analysis of Concrete Frames, ASCE journal, V. 99, LST 8, August, 1973.
5) Berwanger, C. : Limit Design by Successive Moment Distribution, ASCE, Vol. 92, No. ST 1, Feb., 1966.
6) Wang, C.L. : General Computer Program for Limit Analysis, ASCE, Vol. 89, No. ST 6, Dec., 1963.
7) Hognestad, E. : A Study of Combined Bending and Axial load in Reimforced Concrete Members, Bulletin of University of Illinois Engineering Experimental Station, No. 399, Nov., 1951.
8) Beautait, F. and R. R. Williams : Experimental Study of Reinforced concrete Frames Subjected to Alternating Sway Forces, ACI journal, V. 65, pp. 980~984, 1968.
9) Ferdinand L. "Singer, Strength of materials".
10) Ernst, G.C. : Moment and Shear Redistrribution in Two-span Continuous Reinforced Concrete Beams, ACI journal, V. 30, pp. 573~589, 1958.
11) Ernst, G. C., G. M. Smith, A. R. Riveland, and D. N. Pierce : Basic Reinforced Concrete Frame Performance under Vertical and Lateral Loads, ACI journal, V. 70, pp. 261~269, 1973.
12) Gurfinkel, G. and Arthur Robinson : Determination of Strain Distribution and Curvature in a Reinforced Concrete Section Subjected to Bending Moment and Longitudinal Load, ACI journal, V. 64, pp. 398~402, 1967.
13) Sawyer, H.A. : Design of Concrete Frames for Two Failure Stages, Proc. of the International Symposium on Flexural Mechanics of Reinforced Concrete, Miami, Fla., Nov., 1964.
11) Sargin, M. : Stress-strain Relationships for Concrete and the Analysis of Structural Concrete Sections.
15) Park, R. and T. Paulay : Reinforced Concrete Structures, Tohii Wilsy & Sons.
16) Corley, W.G. : Rotational Capacity of Reinforced Concrete Beams, ASCE journal, V. 92, pp. 121~146, 1966.

(Recived August 7, 1978)